Spatial Structure of an Individual Mn Acceptor in GaAs

A. M. Yakunin,[1] A. Yu. Silov,[1] P. M. Koenraad,[1] J. H. Wolter,[1] W. Van Roy,[2] J. De Boeck,[2] J.-M. Tang,[3] and M. E. Flatté[3]

[1]*COBRA Inter-University, Eindhoven University of Technology, P.O. Box 513, NL-5600MB Eindhoven, The Netherlands*

[2]*IMEC, Kapeldreef 75, B-3001 Leuven, Belgium*

[3]*Optical Science and Technology Center and Department of Physics and Astronomy, University of Iowa, Iowa City, Iowa 52242, USA*

(Received 27 January 2004; published 28 May 2004)

The wave function of a hole bound to an individual Mn acceptor in GaAs is spatially mapped by scanning tunneling microscopy at room temperature and an anisotropic, crosslike shape is observed. The spatial structure is compared with that from an envelope-function, effective mass model and from a tight-binding model. This demonstrates that anisotropy arising from the cubic symmetry of the GaAs crystal produces the crosslike shape for the hole wave function. Thus the coupling between Mn dopants in GaMnAs mediated by such holes will be highly anisotropic.

DOI: 10.1103/PhysRevLett.92.216806 PACS numbers: 73.20.–r, 71.55.Eq, 75.50.Pp

Despite intense study of deep acceptors in III-V semiconductors such as Mn_{Ga}, little information has been obtained on their electronic properties at the atomic scale. Yet the spatial shape of the Mn acceptor state will influence hole-mediated Mn-Mn coupling and thus all of the magnetic properties of hole-mediated ferromagnetic semiconductors [1] such as $Ga_{1-x}Mn_xAs$. Evidence for anisotropic spatial structure even in shallow acceptors in various III-V semiconductors [2–5] suggests that anisotropic hole states may be common. In addition to controlling interdopant properties such as the Mn-Mn coupling [6–8], the wave function shape would affect single-dopant properties such as the g factor and optical transition oscillator strengths.

This Letter presents an experimental and theoretical description of the spatial symmetry of the Mn acceptor wave function in GaAs, and we suggest our results imply similar behavior for other acceptors and other hosts. We first present our measurements of the spatial mapping of the anisotropic wave function of a hole localized at a Mn acceptor. To achieve this, we have used the STM tip not only to image the Mn acceptor but also to manipulate its charge state A^0/A^- at room temperature, as described in [9]. Within an envelope-function, effective mass model (EFM) the anisotropy in the acceptor wave function can be traced to differing amplitudes of envelope functions with the same total angular momentum ($L > 0$) but different angular momentum projections along a fixed axis. We introduce into the EFM a single parameter η that describes the breaking, by the cubic crystal, of spherical symmetry for the acceptor level envelope functions. As η has a negligible effect on the binding energy compared to the central cell correction, common variational approaches cannot be used to evaluate η. However, comparison with calculations based on a tight-binding model (TBM) for the Mn acceptor structure [8] permits us to clearly identify the physical origin of the anisotropic shape in these models and to justify the value of η used in our EFM calculations to describe the experimental shape. The TBM calculations also demonstrate that although the spin-orbit interaction does influence the acceptor wave function, the qualitative anisotropic shape of the acceptor state occurs in crystals without spin-orbit interaction. Thus acceptor levels in crystals such as GaN should have a similar shape.

The measurements were performed on several samples using chemically etched tungsten tips. The samples consisted of a 1200 nm thick layer of GaAs doped with Mn at 3×10^{18} cm^{-3} grown by molecular beam epitaxy (MBE) on an intrinsic (001) GaAs substrate. A growth temperature of 580 °C was chosen to prevent the appearance of structural defects such as As antisites, which would complicate the spatial mapping by shifting the position of the Fermi level of the sample. The concentration of the Mn dopants was low enough to neglect Mn-Mn interactions and the formation of an impurity band. The samples we used were insulating below 77 K. The experiments were performed in a room temperature ultrahigh vacuum STM ($P < 2 \times 10^{-11}$ Torr) on an *in situ* cleavage induced (110) surface.

A major advantage to our approach is that the occupation of the acceptor state can be influenced by band bending from the voltage applied between the STM tip and the sample (see inset of Fig. 1). We studied the voltage dependent appearance of the Mn acceptor in the STM constant-current image. In the ionized configuration at high negative bias, Mn appeared as an isotropic round elevation, which is a consequence of the influence of the A^- ion Coulomb field on the valence band states [Fig. 2(a)]. This agrees with a recent study of the individual Mn in GaAs in the ionized configuration [10]. We found that at a positive bias Mn is electrically neutral, as can be seen from the absence of the electronic contrast at high positive voltage ($U > 1.5$ V) when the conduction band empty states dominate tunneling [see the positive branch of the $I(V)$ curve in Fig. 1]. At low positive voltage where the tip Fermi level is below the conduction band edge, Mn appeared as a highly anisotropic crosslike

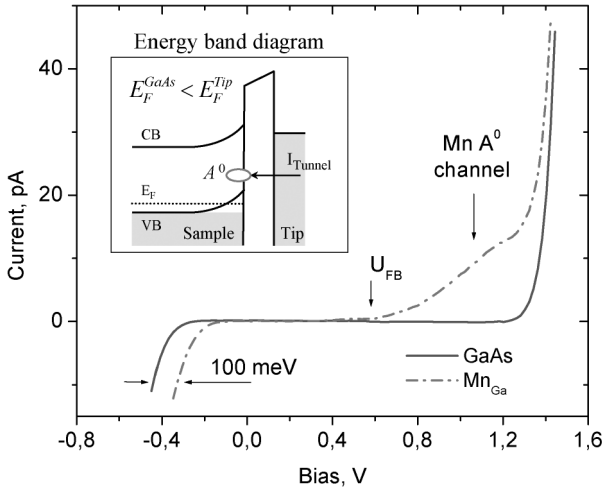

FIG. 1. $I(V)$ curves acquired on the clean GaAs surface (solid line) and in the middle of the crosslike feature (dashed line). The simulated position of the flat-band potential U_{FB} is indicated by the labeled arrow. Inset displays energy band diagram for the positive sample bias.

feature [Figs. 2(b) and 3(a)]. The anisotropy is even more evident in a reciprocal-space image [Fig. 3(b)]. The methods of calculating the theoretical images [Figs. 2(d) and 3(c)–3(f)] will be described below.

The crosslike feature manifested itself in the local tunneling $I(V)$ spectroscopy at low voltages when the GaAs bands do not contribute to the tunneling. It appeared as an empty states or filled states current channel in the band gap of GaAs depending on applied positive or negative bias, respectively. Thus the mapping of the Mn acceptor state in the filled (empty) states mode was realized by electron (hole) injection into the A^0/A^- state. In the tunneling $I(V)$ spectroscopy, the manganese A^0 channel appeared presumably above the flat band potential U_{FB} and was available for tunneling in the wide range of voltages above U_{FB}. Our estimated value of U_{FB} is about $+0.6$ V. The observed ionization energy, which was determined from the shift of the $I(V)$ spectrum at negative bias, corresponds to the Mn acceptor binding energy $E_a = 0.1$ eV.

The concentration of the dopants we observed with STM corresponds to the intentional 3×10^{18} cm^{-3} doping level. In the experiment we identified Mn located in at

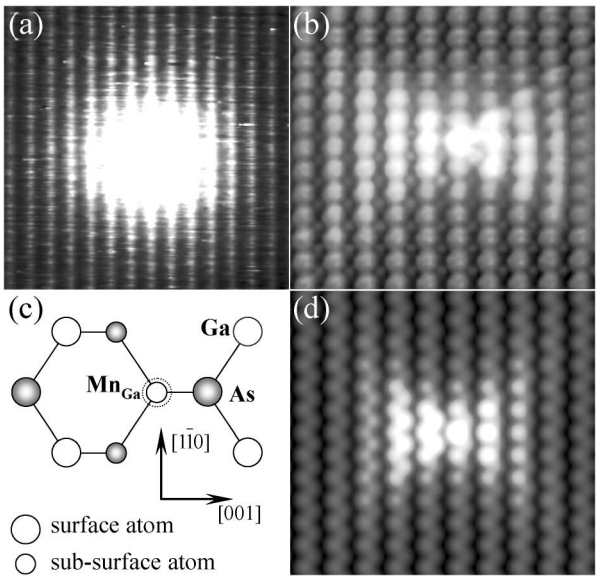

FIG. 2. (a) 8×8 nm^2 STM image of an ionized Mn acquired at -0.7 V. (b) 5.6×5 nm^2 STM image of neutral Mn acquired at $+0.6$ V. Big and small round features correspond to As and Ga related surface states, respectively. Presumably, Mn is located in third subsurface atomic layer. (c) A model of the (110) surface (top view) representing the Mn on Ga site located in an odd subsurface atomic layer (counting surface layer as zero). (d) 5.6×5 nm^2 simulated image (logarithm of local density of states) of the Mn located in the fifth subsurface atomic layer (TBM).

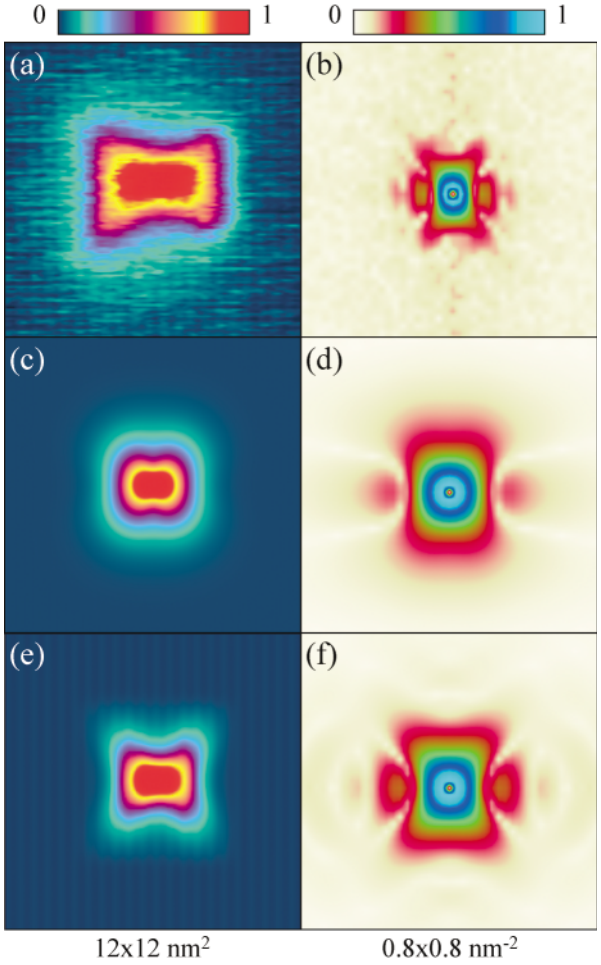

FIG. 3 (color). (a) Constant-current image of the neutral Mn acquired at $+0.9$ V. Mn is presumably located in the second subsurface atomic layer. (b) Fourier spectrum of image (a). (c) Simulated image of the Mn acceptor ground state $1S_{3/2}$ (EFM). (d) Fourier spectrum of image (c). (e) Simulated image of the Mn acceptor density of states (TBM). (f) Fourier spectrum of image (e). Images (c) and (e) were simulated assuming Mn to be located in the fourth subsurface atomic layer.

least six different layers under the surface. In order to determine the actual position of the Mn dopants, we analyzed the intensity of the electronic contrast of the Mn related features. Based on the symmetry of the crosslike feature superimposed on the surface lattice, we distinguished whether the dopant is located in an even or odd subsurface layer. We found that at any depth the shape of the hole on the (110) surface had nearly C_{2v} symmetry around the surface normal and was elongated along the [001] direction relative to the $[1\bar{1}0]$ direction. The crosslike features induced by deeper dopants were more elongated in the [001] direction. The feature was weakly asymmetric with respect to the $[1\bar{1}0]$ direction [lowering the symmetry to the single $(1\bar{1}0)$ mirror plane], which may come from the symmetry properties of the (110) surface.

A four-band envelope-function effective Luttinger-Kohn Hamiltonian provided one framework (EFM) in which to analyze the spatial structure of the bulklike neutral acceptor complex formed by a valence hole loosely bound to a negatively charged $Mn^{2+}3d^5$ core ($Mn^{2+}3d^5$ + hole complex). We neglected possible effects caused by the presence of the (110) surface and quantum spin effects from the exchange interaction between the $Mn3d^5$ core and the hole. We also ignored excited states, as the energy separation between the ground state $E_a(1S_{3/2}) = 113$ meV and the first excited state $E_a(2S_{3/2}) = 25$ meV exceeds room temperature [11].

According to Ref. [12], the acceptor wave function in zinc blende semiconductor is represented as a four-component column written in the basis of Bloch functions of the valence band top Γ_8. The form of the wave function component $\psi^{3/2}_{3/2}(\theta, \varphi, r)$ is proportional to

$$R_0\begin{Vmatrix} Y_{0,0} \\ 0 \\ 0 \\ 0 \end{Vmatrix} + c^{F_1}R_2\begin{Vmatrix} 0 \\ 2Y_{2,1} \\ Y_{2,2} - Y_{2,-2} \\ 0 \end{Vmatrix} + c^{E}R_2\begin{Vmatrix} \sqrt{2}Y_{2,0} \\ 0 \\ Y_{2,2} + Y_{2,-2} \\ 0 \end{Vmatrix}, \tag{1}$$

where

$$c^E/c^{F_1} = \eta, 0 \le \eta \le 1, \tag{2}$$

$Y_{L,m}(\theta, \varphi)$ are spherical harmonics, $R_L(r)$ are radial parts of the envelope functions, and c^E and c^{F_1} are the constants described below.

As pointed out by Schechter and Kohn [13,14], in this model $R_L(r)Y_{L,m}(\theta, \varphi)$ are eigenfunctions of parity. Thus the wave function [Eq. (1)] contains only even s-like ($L = 0$) and d-like ($L = 2$) components. In Eq. (1) the angular part of the d-component includes components which transform according to the Γ_{12} and Γ_{25} representations of the tetrahedral point group. Their corresponding coefficients are the constants c^E and c^{F_1}, respectively, whose ratio is denoted here as η [Eq. (2)].

The value of η depends on the valence band parameters of the particular material and could be evaluated variationally from the binding energy [12–14]. However, the introduction of η only weakly effects the binding energy and is negligible compared to a central cell correction. To clarify the nature of the Mn acceptor ground state, here we used η as a free parameter, and thus varied the spherical anisotropy from $\eta = 1$, corresponding to a completely spherically symmetric solution, till $\eta \to 0$, where the E component vanished. When $\eta = 1$, the function [Eq. (1)] transforms to that one obtained by Baldereschi and Lipari in the spherical approximation [15].

Although the EFM describes the symmetry of the Mn acceptor, it fails to predict the ground-state binding energy E_0 without a central cell correction [16]. Deep acceptors such as Mn in GaAs are usually described by the zero-range potential model [17,18]. In this model the spatial extension of the wave function depends on a parameter α, determined by E_0:

$$\alpha = \frac{\sqrt{2m_hE_0}}{\hbar}\left(\frac{\beta\sqrt{\beta}+1}{\beta+1}\right), \qquad \beta = \frac{m_l}{m_h}, \tag{3}$$

where α defines the spatial localization of the hole trapped at the acceptor with a binding energy E_0 and β is the ratio of light to heavy hole masses. For GaAs we used $\alpha = 1.197\ \mathrm{nm}^{-1}$ and $\beta = 0.132$, as in Refs. [7,15]. This model allows one to obtain analytical expressions for $R_0(r)$ and $R_2(r)$ [18]. The admixture of the d-like component to the ground-state, calculated by Baldereschi and Lipari [15] for GaAs, is 30% and corresponds to what we have found using the zero-range potential model. As can be seen from Ref. [18], the d-like component dominates at distances $R > 1/\alpha$. The admixture of higher orbital momentum will vanish in the limit $\beta \to 1$. In the case $\beta = 0$, the envelope functions R_0 and R_2 can be derived in an implicit form [19]. In Ref. [19] authors emphasize the different behavior of R_0 and R_2 at large distances. The R_0 drops exponentially whereas R_2 has power law decay at infinity.

In Fig. 3(c) we present the cross section of the bulklike charge density of the total wave function in the limit case $\eta = 0$ cut through an imaginary (110) plane at the distance of 0.8 nm from the Mn position. The plot is presented with a logarithmic scale because of the inverse exponential dependence of the tunnel current on the tip-sample distance during the actual STM experiment. Figure 3(d) presents the calculated Fourier transform. Note the presence of the satellite harmonics that arise from the steep fall off of the wave function in the [001] direction. The model reproduces the key symmetry elements in the Fourier spectra: the elongation of the spectra along $[1\bar{1}0]$ direction, the satellites in [001] direction, and the crosslike shape. However, the crosslike shape and the intensity of the satellites are more pronounced in the experimental Fourier spectrum. Based on the analyses we performed, we conclude that only the harmonic $Y_{2,1}$ gives rise to the intensity of the satellites in the Fourier spectrum.

The tight-binding model we use [8] is based on the deep level model of Vogl and Baranowski [20]. The

dangling sp^3 bonds from the nearest-neighbor As hybridize with the Mn d-states of Γ_{15} character. The antibonding combination of these becomes the Mn acceptor state. Coupling to the d-states of Γ_{12} character is weak, and hence neglected. The hybridization strength is fully determined by the acceptor level energy. This model, if further approximated within the EFM, predicts $\eta = 0$, similar to what we found by fitting the EFM to the experimental measurements.

The calculations of the local density of states (LDOS) based on the TBM are shown in logarithmic scale in Figs. 2(d), 3(e), and 3(f). The results show symmetry under reflection in the $(1\bar{1}0)$ plane and asymmetry under reflection in the (001) plane. For Mn dopants several layers down from the surface, as in Fig. 2(b), the shape of the acceptor state does not depend that sensitively on the spin orientation of the Mn-core $3d$ spin. For these dopants the shape does not depend on the spin-orbit interaction; we confirmed this by obtaining a similar crosslike acceptor structure using a tight-binding Hamiltonian without spin-orbit interaction and with empirical parameters designed for optimal agreement with the bulk band structure of GaAs [21]. The situation differs greatly for Mn near the surface, where the axis of extension of the acceptor state rotates with the spin orientation of the Mn-core spin. At these temperatures we can expect the Mn-core spin to point in a random direction and for the STM measurements to average over the possible spin orientations. Thus for Figs. 2(d), 3(e), and 3(f) the LDOS is averaged over the Mn spin orientation.

Although the symmetry is well retained for all simulated positions of Mn under the surface, in both models the best fits were achieved when the apparent depth of the Mn is assumed to be two atomic layers larger. The reason for this could be the vacuum barrier, which will tend to shift the wave function of the Mn acceptor state deeper into the crystal than one would predict for the sliced bulk crystal calculation. The lateral size of the wave function measured is also somewhat larger than calculated for Fig. 3; this might come from a reduction of the acceptor binding energy very near the surface.

In conclusion, we have experimentally demonstrated that the Mn acceptor ground state has highly anisotropic spatial structure. This spatial anisotropy is due to a significant presence of d-wave envelope functions in the acceptor ground state. We have demonstrated that the observed symmetry can be explained within a simple tight-binding model, whose only free parameter is the acceptor level energy. We also found that this spatial structure can be described well by a simple four-band envelope-function model of cubic symmetry, whose key parameter, η, can be fit to the observed spatial structure and is similar to that expected from a tight-binding model. These results have broad implications for all acceptor-acceptor interactions in zinc blende semiconductors and especially for hole-mediated ferromagnetic semiconductors.

This work was supported by the Dutch Foundation for Fundamental Research on Matter (FOM), the Belgian Fund for Scientific Research Flanders (FWO), the EC GROWTH Project FENIKS (Project No. G5RD-CT-2001-00535), and the ARO Grant No. MURI DAAD-19-01-1-0541.

[1] H. Ohno, in *Semiconductor Spintronics and Quantum Computation*, edited by D. D. Awschalom, N. Samarth, and D. Loss (Springer, Berlin, 2002).
[2] Z. F. Zheng, M. B. Salmeron, and E. R. Weber, Appl. Phys. Lett. **64**, 1836 (1994); **65**, 790(E) (1994).
[3] R. de Kort, M. C. M. M. van der Wielen, A. J. A. van Roij, W. Kets, and H. van Kempen, Phys. Rev. B **63**, 125336 (2001).
[4] T. C. G. Reusch, M. Wenderoth, L. Winking, R. G. Ulbrich, G. Döhler, and S. Malzer, in *Proceedings of the 12th International Conference on Scanning Tunneling Microscopy/Spectroscopy and Related Techniques, Eindhoven, The Netherlands, 2003*, edited by P. M. Koenraad, Abstract No. Tu-8-C3.
[5] P. I. Arseev, N. S. Maslova, V. I. Panov, S. V. Savinov, and C. Van Haesendock, JETP Lett. **77**, 172 (2003).
[6] G. Zaránd and B. Jankó, Phys. Rev. Lett. **89**, 047201 (2002).
[7] G. A. Fiete, G. Zaránd, and K. Damle, Phys. Rev. Lett. **91**, 097202 (2003).
[8] J.-M. Tang and M. E. Flatté, Phys. Rev. Lett. **92**, 047201 (2004).
[9] A. M. Yakunin, A. Yu. Silov, P. M. Koenraad, W. Van Roy, J. De Boeck, and J. H. Wolter, Physica (Amsterdam) **21E**, 947 (2004).
[10] T. Tsuruoka, R. Tanimoto, N. Tachikawa, S. Ushioda, F. Matsukura, and H. Ohno, Solid State Commun. **121**, 79 (2002).
[11] M. Linnarsson, E. Janzén, B. Monemar, M. Kleverman, and A. Thilderkvist, Phys. Rev. B **55**, 6938 (1997).
[12] G. L. Bir and G. E. Pikus, in *Symmetry and Strain-Induced Effects in Semiconductors* (Halsted, Jerusalem, 1974).
[13] D. Schechter, J. Phys. Chem. Solids **23**, 237 (1962).
[14] W. Kohn and D. Schechter, Phys. Rev. **99**, 1903 (1955).
[15] N. O. Lipari and A. Baldereschi, Phys. Rev. Lett. **25**, 1660 (1970); A. Baldereschi and N. O. Lipari, Phys. Rev. B **8**, 2697 (1973).
[16] A. K. Bhattacharjee and C. Benoit á la Guillaume, Solid State Commun. **113**, 17 (2000).
[17] V. I. Perel' and I. N. Yassievich, Zh. Eksp. Teor. Fiz. **82**, 237 (1982) [Sov. Phys. JETP **55**, 143 (1982)].
[18] N. S. Averkiev and S. Yu. Ilyinskii, Fiz. Tverd. Tela (Leningrad) **36**, 503 (1994) [Phys. Solid State **36(2)**, 278 (1994)].
[19] T. L. Linnik and V. I. Sheka, Phys. Solid State **41**, 1425 (1999).
[20] P. Vogl and J. M. Baranowski, Acta Phys. Pol. A **67**, 133 (1985).
[21] D. J. Chadi and M. L. Cohen, Phys. Status Solidi B **68**, 405 (1975).